EINDHOVEN UNIVERSITY OF TECHNOLOGY

Fully Integrated, 80 GHz Bandwidth, 1.3μ m InAs/InGaAs CW-PW Quantum Dot Passively Colliding-Pulse Mode-Locked (CPM) Lasers for IR Sensing Application

Citation for published version (APA):
Heydari, M., Rasoulzadehzali, A., Esmailpour Gildeh, R., & Farmani, A. (2022). Fully Integrated, 80 GHz Bandwidth, 1.3μ m InAs/InGaAs CW-PW Quantum Dot Passively Colliding-Pulse Mode-Locked (CPM) Lasers for IR Sensing Application. *IEEE Sensors Journal*, *22*(7), 6528-6535. https://doi.org/10.1109/JSEN.2022.3153656

Document license:
TAVERNE

DOI:
10.1109/JSEN.2022.3153656

Document status and date:
Published: 01/04/2022

Document Version:
Publisher's PDF, also known as Version of Record (includes final page, issue and volume numbers)

Please check the document version of this publication:

• A submitted manuscript is the version of the article upon submission and before peer-review. There can be important differences between the submitted version and the official published version of record. People interested in the research are advised to contact the author for the final version of the publication, or visit the DOI to the publisher's website.
• The final author version and the galley proof are versions of the publication after peer review.
• The final published version features the final layout of the paper including the volume, issue and page numbers.

Link to publication

General rights
Copyright and moral rights for the publications made accessible in the public portal are retained by the authors and/or other copyright owners and it is a condition of accessing publications that users recognise and abide by the legal requirements associated with these rights.

• Users may download and print one copy of any publication from the public portal for the purpose of private study or research.
• You may not further distribute the material or use it for any profit-making activity or commercial gain
• You may freely distribute the URL identifying the publication in the public portal.

If the publication is distributed under the terms of Article 25fa of the Dutch Copyright Act, indicated by the "Taverne" license above, please follow below link for the End User Agreement:

www.tue.nl/taverne

Take down policy
If you believe that this document breaches copyright please contact us at:

openaccess@tue.nl

providing details and we will investigate your claim.

Download date: 04. Oct. 2023

IEEE Sensors Council

Fully Integrated, 80 GHz Bandwidth, 1.3 μm InAs/InGaAs CW-PW Quantum Dot Passively Colliding-Pulse Mode-Locked (CPM) Lasers for IR Sensing Application

Mohammad Heydari, Aref Rasoulzadeh Zali, Reza Esmailpour Gildeh, and Ali Farmani, *Member, IEEE*

***Abstract*—Integrated quantum dot passively mode-locked lasers: IQDMLLs open opportunities for IR sensing. Therefore, here, we investigated structure of quantum dot passively mode-locked lasers (QDMLLs) with colliding-pulse mode-locked (CPM) method in order to reinforce the performance of QDMLLs for ultrahigh-bit-rate compared to self-colliding pulse mode-locking (SCPM) method. The proposed structure is numerically based on finite difference traveling wave (FDTW) method. By considering bias current of 80 mA, which is the bias applied to the gain section, the laser is at its maximum output power. Finally, by comparing the QDMLLs with self-colliding pulse mode-locking (SCPM) method, it is shown that due to the grating caused by the collision of the two counter-propagating pulses in the saturable absorber, the laser bit rate in the structure of CPM is twice the bit rate in structure of SCPM somehow bit rate from 40 GHz in SCPM method increased to 80 GHz in CPM method. Also, grating coupling factor (GCF) changes due to the proposed structure has been shown, so that in the range of 1cm^{-1} $\leq \kappa \leq$ 5cm^{-1} the laser output power is pulsed wave (PW), while after this range the laser output power changes from a pulsed regime to a continuous wave (CW) regime.**

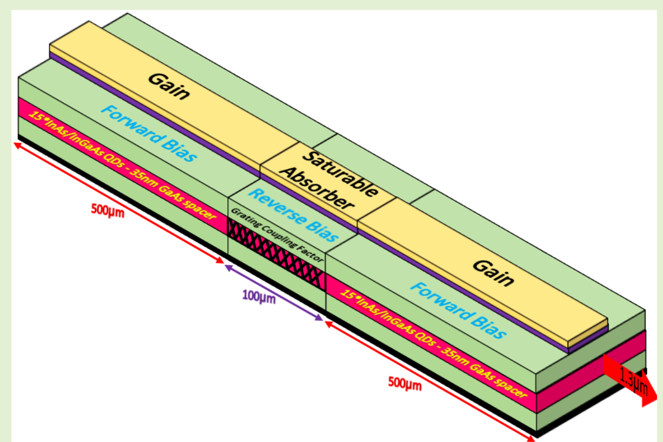

***Index Terms*— IR sensing, quantum dot passively mode-locked lasers (QDMLLs), colliding-pulse mode-locked (CPM), self-colliding pulse mode-locking (SCPM), saturable absorber, grating coupling factor (GCF).**

I. Introduction

DUE to recent advances in optical systems, for instance, 5G and 6G system networks, artificial intelligence (AI) in optical communication [1], Internet of Things (IoT) based on optical technologies [2], the need for short optical pulses with very high bit rates have been considered for applications such as increasing the bandwidth of transmitters, and optical receivers, converters, optical communications and medical [3], [4]. One of the most critical applications of short-pulse lasers in medicine and imaging is in the near-infrared (NIR) wavelength range. The approximate NIR wavelength is 0.7 μm to 2.5 μm. Since the 0.7 μm to 1.3 μm wavelength is an optical window, it has many medical applications, especially in biomedical imaging such as optical coherence tomography (OCT), due to its deep penetration depth into tissues. Using these resources to image human skin requires a wavelength of 1.3 μm, which is possible using InAs self-assembled quantum dots(QDs). InAs QDs are an excellent candidate for the NIR region due to their constructional and sizing characteristics. Therefore, infrared emission and detection are possible in many applications using InAs/InGaAs quantum dot lasers [5]–[7]. Q-switching, gain switching, and mode-locking (ML) are three main approaches to produce light pulses [8], [9]. The most widely used method for producing high-intensity, short-width pulses is Q-switching. The use of

Manuscript received February 7, 2022; accepted February 20, 2022. Date of publication February 22, 2022; date of current version March 31, 2022. The associate editor coordinating the review of this article and approving it for publication was Ms. Shiva Abbaszadeh. *(Corresponding author: Ali Farmani.)*

Mohammad Heydari and Reza Esmailpour Gildeh are with the Nano-Photonic Research Group, Faculty of Engineering, Shahed University, Tehran 1411713116, Iran (e-mail: mohammad.heydari@shahed.ac.ir; r.esmailpourgildeh@shahed.ac.ir).

Aref Rasoulzadeh Zali is with the Department of Electrical Engineering, IPI-ECO Research Institute, Eindhoven University of Technology, 5612 AZ Eindhoven, The Netherlands (e-mail: a.rasoulzadehzali@tue.nl).

Ali Farmani is with the Optoelectronic Research Center, Department of Electrical and Computer Engineering, Lorestan University, Khorramabad 68151-44316, Iran (e-mail: farmani.a@lu.ac.ir).

Digital Object Identifier 10.1109/JSEN.2022.3153656

1558-1748 © 2022 IEEE. Personal use is permitted, but republication/redistribution requires IEEE permission. See https://www.ieee.org/publications/rights/index.html for more information.

Authorized licensed use limited to: Eindhoven University of Technology. Downloaded on June 20,2022 at 13:21:18 UTC from IEEE Xplore. Restrictions apply.

this method has been reported on a silicon substrate with a wavelength of 1.3 μm [10]. On the other hand, the use of Q-switching to achieve dual wavelengths, which is used in a wide range of applications such as optical communication and precision spectroscopy, has been investigated in Yb: LuYAG and Nd: GSAG lasers. Nd: GSAG laser using saturable absorber molybdenum disulfide (MoS_2) is a passive type that can be implemented in low-cost integrated applications, has been reported for the first time to achieve dual-wavelength, and has received much attention. As with Q-switching, access dual wavelengths using the mode-locked method in a recently proposed erbium-doped fiber laser demonstrates the capability of the mode-locked method [11], [12]. ML method is the most crucial technique for generating consecutive pulses [13]. The gain switching and Q-switching methods are used in the transient mode of the laser, while the ML method is used in the steady-state laser mode. The generated pulses have less noise than the transition pulses and a much shorter width at the output [14]. Semiconductor lasers based on self-assembled QDs are especially suitable for the ML regime [15]. As with Q-switching, access dual wavelengths using the ML method in a recently proposed erbium-doped fiber laser demonstrates the capability of the ML method [16]. Their unique properties include the high-speed dynamics of the carriers as well as the extensive bandwidth, and absorption band are of particular importance in the production of very short pulses [17]. There are two major models for simulating mode-locked lasers (MLLs), the finite difference traveling waves (FDTWs) and delay differential equations (DDEs) methods [18]–[21]. FDTW is an efficient method we use because it has higher accuracy and the ability to simulate real effects such as spontaneous emission noise [22], [23]. The proposed structure in this paper has several essential features that distinguish it from other structures such as distributed feedback quantum dot passively mode-locked lasers (DFB-QMLLs), grating-embedded saturable absorber distributed feedback quantum dot passively mode-locked lasers (GESA-DFB-QDMLL), and SCPM. One of the most critical differences in the designed structure is the high output frequency and low bias current applied to the gain section, making this structure desirable in integrated circuit applications. The proposed structure increases the laser output frequency to 80 GHz. This subject is important because this is done using a virtual grating according to the structure designed and the collision of counter-propagating pulses in the saturable absorber (SA) for the quantum dot laser. Furthermore, the output power in the range of milliwatts and the output wavelength of 1.3 μm makes this laser ideal for NIR diagnostic applications and integration. On the other hand, the mirrors symmetry and the reduction of the laser length in the structure of the paper will reduce the effect of longitudinal spatial hole burning (LHSB), which is vital in the design of lasers.

II. Structure

The proposed structure consists of two gain regions and a saturable absorber (SA) region bounded by two gain regions, as shown in Fig. 1. Waveguide absorbers and semiconductor saturable absorber mirrors (SESAM) are two common types of saturated adsorbents that use the second type of adsorbent in this structure. These absorbers are integrated into a mirror structure; Bragg mirrors and their work are usually reflections. The structure presented in this part, unlike Ref. [4], which has an asymmetric design and the total length of the laser is 3mm, the left gain section is 700 μm, the right part is 1600 μm and the absorber is 700 μm, which has a repetition rate of 13.24 GHz while The structure shown in Fig. 1 is a symmetrical structure with a length of 500 μm for each of the gain sections and 100μm for the SA section, with a repetition rate of 80GHz at the output. Both sides of the laser here are of partial reflection type and have a reflection coefficient of $\sqrt{0.495}$, which is the most optimal output power in these conditions. The gain regions have a forward-biased and the SA region includes a reverse-biased. Also, unlike Ref. [4], where the applied current is between 75 mA to 1100 mA, in this structure, the laser applied current is from 1 mA to 130 mA, which is much less current than the Ref. [4] structure. All three Q-switching regimes, Pulse and continuous regimes occur in this range. The active region of the laser consists of 15 layers of InAs/InGaAs QDs [27]. Furthermore, the wave created in the SA section is a standing wave due to the collision of two traveling waves in this region. This is shown in Fig. 2.

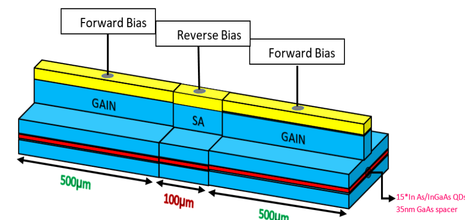

Fig. 1. Schematic of quantum dot mode-locked laser with CPM technique.

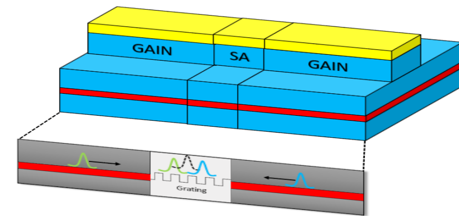

Fig. 2. Side view of the laser and how to form a standing wave in the SA.

III. Equations

This section examines the equations of the optical emission fields within the laser cavity, the carrier density, and the boundary conditions. To simulate the structure, we need to express optical emission fields, propagating constant, boundary conditions, carrier density, and recombination concepts. In this section, by examining the equations of the device, a detailed analysis of how it works to be provided.

A. Field Equations

The longitudinal propagation of the transverse mode of the electromagnetic field within the laser cavity is derived from

Authorized licensed use limited to: Eindhoven University of Technology. Downloaded on June 20,2022 at 13:21:18 UTC from IEEE Xplore. Restrictions apply.

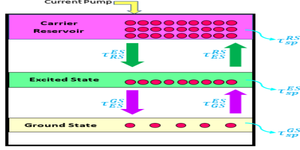

Fig. 3. Internal structure of the GAIN section.

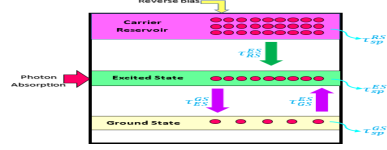

Fig. 4. Internal structure of the SA section.

a time-domain model for DFB semiconductor lasers in which the forward and backward traveling wave equations of the field are described using a counter-propagating electric field [26], [32]. Considering the grating coupling factor (GCF) in the field equation in the CPM structure for a QD laser is the first to occur.

$$\frac{\delta}{\delta t}E^+(z,t) = v_g(-\frac{\delta}{\delta z} - i\beta)E^+(z,t) + SP^+(z,t) - i\kappa_{E^-\to+}E^-(z,t) \quad (1)$$

$$\frac{\delta}{\delta t}E^-(z,t) = v_g(+\frac{\delta}{\delta z} - i\beta)E^-(z,t) + SP^-(z,t) - i\kappa_{E^+\to-}E^-(z,t) \quad (2)$$

where $E^+(z,t)$, $E^-(z,t)$ are the complex amplitude for forward and reverse optical field, which t is time, and z is longitudinal direction, and is in the range 0 to L, which is along the length of the laser cavity. $SP^+(z,t)$ and $SP^-(z,t)$ indicates spontaneous emission noise. Also, $\kappa_{E^-\to+}$ and $\kappa_{E^+\to-}$ in the above equations are grating coupling factor (GCF), β is propagating factor and is expressed as follows [24].

$$\beta = \beta(n_{GS}(z,t),z) = \delta - i\frac{\alpha}{2} + \frac{(i-\alpha_H)}{2}g'(2n_{GS}-1) \quad (3)$$

where δ is static detuning factor. α and α_H indicates the internal absorption, the linewidth enhancement factor. Also g' and n_{GS} denote the effective differential gain and ground-state carrier probability. In this paper, because of the non-uniform broadcast of QDs, the inhomogeneous broadening is not considered, and the Lorentzine profile is used for simulation [17], [27]–[30].

$$E^+(0,t) = r_0E^-(0,t) \quad (4)$$

$$E^-(L,t) = r_LE^+(L,t) \quad (5)$$

where, r0 and rL indicate reflection coefficient of the laser facets.

B. Carrier Rate Equations

Since the laser consists of three parts, the gain regions are located on the sides, and the absorber region is between the gain regions; thus, we will use two rate equations. One set will be for the gain zone, and the other will be for the adsorbent zone. The difference in the carrier rate equations in gain and SA is due to the different gain and SA regions biases. Eqs. 6-8 represent the carrier rate equations in the gain section. The corresponding figure for expressing the internal structure of the gain section and how the carriers interact between the three levels of the ground, excited, and reservoir carriers are shown in Fig. 3. Also, The corresponding figure for the carrier interaction and how the carrier levels are positioned for the SA section is shown in Fig. 4 [27], [31].

$$\frac{d}{dt}n_{GS}(z,t) = -\frac{n_{GS}}{\tau_{GS}} + \frac{2n_{ES}(1-n_{GS})}{\tau_{ES}^{GS}} - \frac{n_{GS}(1-n_{ES})}{\tau_{GS}^{ES}} - R_{st}(n_{GS},E) \quad (6)$$

$$\frac{d}{dt}n_{ES}(z,t) = -\frac{n_{ES}}{\tau_{ES}} - \frac{n_{ES}(1-n_{GS})}{\tau_{ES}^{GS}} + \frac{n_{GS}(1-n_{ES})}{2\tau_{GS}^{ES}} + \frac{n_{CR}(1-n_{ES})}{4\tau_{CR}^{ES}} - \frac{n_{ES}}{\tau_{ES}^{CR}} \quad (7)$$

$$\frac{d}{dt}n_{CR}(z,t) = \frac{I}{e\theta_I} - \frac{n_{CR}}{\tau_{CR}} - \frac{n_{CR}(1-n_{ES})}{\tau_{CR}^{ES}} + \frac{4n_{ES}}{\tau_{ES}^{CR}} \quad (8)$$

The rate equations for the saturable absorber section using the simplified model of these equations are as follows [20], [22].

$$\frac{d}{dt}n_{GS}(z,t) = -\frac{n_{GS}}{\tau_{GS}} + \frac{2n_{ES}(1-n_{GS})}{\tau_{ES}^{GS}} - \frac{n_{GS}(1-n_{ES})}{\tau_{GS}^{ES}} - R_{st}(n_{GS},E) \quad (9)$$

$$\frac{d}{dt}n_{ES}(z,t) = -\frac{n_{ES}}{\tau_{ES}^{CR}} - \frac{n_{ES}(1-n_{GS})}{\tau_{ES}^{GS}} + \frac{n_{GS}(1-n_{ES})}{2\tau_{GS}^{ES}} \quad (10)$$

$$R_{st}(n_{GS},E) = \frac{1}{\theta_E}\sum_{\upsilon=\pm} E^{\upsilon *}(g'(2n_{GS}-1))E^{\upsilon} \quad (11)$$

where τ_x^y shows spontaneous relaxation and τ_x illustrate transition rates. x,y belong to ground state(GS), exited state (ES) and carrier reservoir (CR). I is injection current to gain section, e is electron charge and θ_I, θ_E are Scaling parameters, Also, Rst is a stimulated recombination.

IV. Simulations and Results

To find the solution of the field and carrier rate equations, it is possible to solve these equations coupled together by using the Runge–Kutta and FDTW method in the MATLAB software [34]. For this purpose, the laser is divided, so that the time axis is divided by the step length dt and the location axis, which is in the direction of the laser length by the step length dz. The relationship between temporal and spatial steps is $dt = dz/v_g$. The output of the proposed laser structure depends on several basic parameters. The current applied to the gain section, the reverse voltage applied to the saturable absorber region, ground-state carrier probability, and also the grating coupling effect (GCE) is the parameters that are examined.

Authorized licensed use limited to: Eindhoven University of Technology. Downloaded on June 20,2022 at 13:21:18 UTC from IEEE Xplore. Restrictions apply.

TABLE I
PARAMETERS USED FOR NUMERICAL SIMULATION [27]

symbol	Quantity	Value
λ_0	Central wavelength	1.3 μm
n_{gr}	Group refractive index	3.75
L	Total length	1mm
δ	Static detuning	0 cm^{-1}
α	Internal absorption	5 cm^{-1}
α_H	Henry factor	2
g'_G	Effective differential gain	40 cm^{-1}
g'_{SA}	Effective differential absorption	200 cm^{-1}
$\bar{g}$	Susceptibility	40 cm^{-1}
$\bar{\omega}$	Susceptibility	20 cm^{-1}
$2\bar{\gamma}$	Susceptibility	0 cm^{-1}
τ_{GS}	GS Relaxation rate	1ns
τ_{ES}	ES Relaxation rate	1ns
τ_{CR}	CR Relaxation rate	1ns
τ_{GS}^{ES}	GS to ES transition time	5ps
τ_{ES}^{GS}	ES to GS transition time	2ps
τ_{CR}^{ES}	CR to ES transition rate (G)	5ps
τ_{CR}^{ES}	CR to ES transition rate (SA)	0
τ_{ES}^{CR}	ES to CR transition rate (G)	80ps
τ_{ES}^{CR}	ES to CR transition rate (SA)	$18e^{U/2V}ps$
θ_I	Injection scaling factor	$9.36 \cdot 10^6$
θ_E	Field scaling factor	239ps
Γ	Transversal confinement factor	0.075
U	reverse-bias voltage SA section facet	[0, -7]
r_0	SA section facet reflectivity	$\sqrt{0.495}$
r_L	Gain section facet reflectivity	$\sqrt{0.495}$

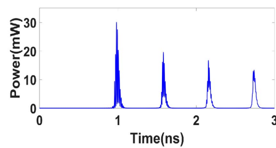

Fig. 5. Q-switching laser mode in 40mA.

A. Current Effect

One of the effective parameters in determining the laser output is the current applied to the gain section. By using the appropriate current to the gain section, and when the current reaches the threshold value, which in this structure is 10 mA, the laser turns on due to spontaneous emission and enters the Q-switching regime as shown in Fig. 5. In this case, the pulses generated at the output are wide, irregular, and unstable. Pulses with a time linewidth of about a few hundred picoseconds and a repetition rate equal to a few hundred MHz are produced at the laser output. By increasing the current to 50 mA, which is the value of the mode-locking threshold current (Fig. 6(a)), the production of ultra-short stable light pulses at the laser output begins. The steady-state time of the laser is about several nanoseconds. As the current increases continuously (Fig.6(b)), the maximum laser output power will not only not increase but also decrease. As the current increases from the start of the mode lock to 80 mA, the maximum output power does not change much, and the output pulse becomes slightly more expansive. But after the middle currents and with the increase of current of the gain area, as seen in Fig. 6(c) and Fig. 6(d), the maximum output power decreases and the desired pulse widens sharply, and finds an extremum. Because with increasing current, the set of modes with less co-phase also finds the necessary power to appear at the maximum output power and appear in the output pulse as extremum. As a result, in this case, the increase in power due to the rise in current is spent on increasing the power of other co-phase modes, and the maximum power is also reduced. A comparison between the output power size and the pulse width is shown in Fig. 6(e) The effect of current change on the wetting layer carrier density is also illustrated in Fig.7. It is observed that increasing the applied current increases the carrier density of the wetting layer. The carrier density has an initial increase value that over time and in a steady-state, we see relatively constant changes in the carrier density.

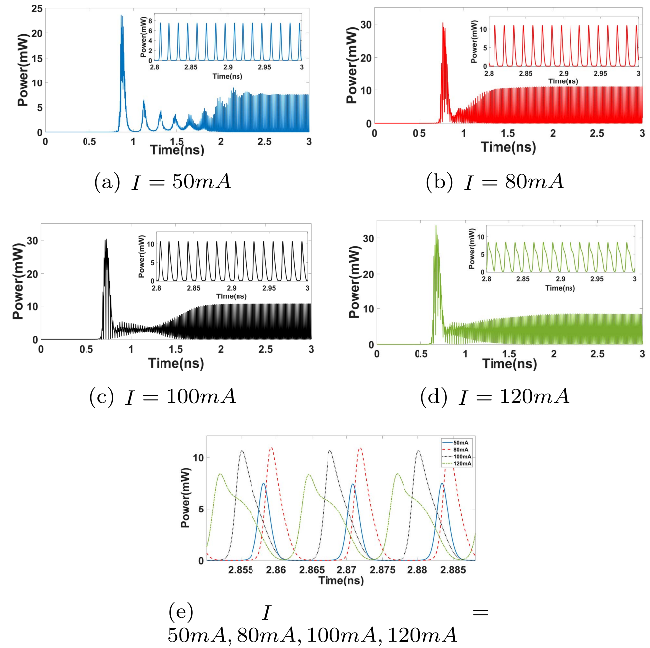

(a) $I = 50mA$ (b) $I = 80mA$ (c) $I = 100mA$ (d) $I = 120mA$ (e) $I = 50mA, 80mA, 100mA, 120mA$

Fig. 6. Output power versus on applied current to the gain section.

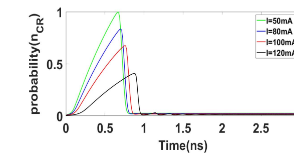

Fig. 7. Current effect on wetting layer carrier density.

B. Voltage Effect

A negative voltage applied to the saturable absorber section is another important parameter that plays a vital role in how the laser works. According to the carrier rate equations related to the absorption region, which are expressed in Eq. 9 and Eq. 10, the carrier relaxation time from the excited state to the wetting layer τ_{ES}^{CR} with the applied voltage to the absorber region is exponential. According to the simulation results of Fig. 8(a) - 8(e), it is clear that the applied voltage

Authorized licensed use limited to: Eindhoven University of Technology. Downloaded on June 20,2022 at 13:21:18 UTC from IEEE Xplore. Restrictions apply.

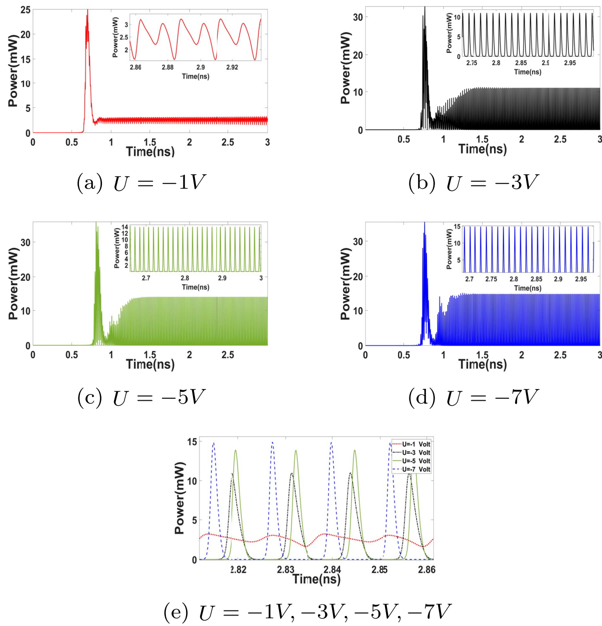

(a) $U = -1V$ (b) $U = -3V$

(c) $U = -5V$ (d) $U = -7V$

(e) $U = -1V, -3V, -5V, -7V$

Fig. 8. Output power versus on reverse voltage to the SA section.

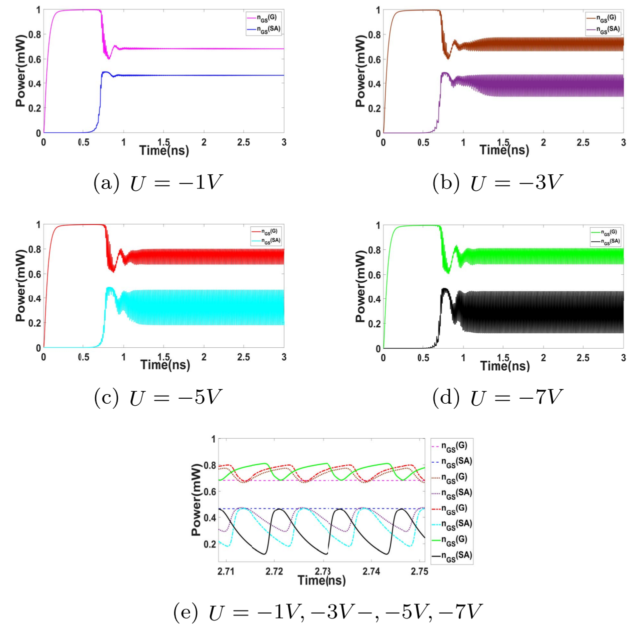

(a) $U = -1V$ (b) $U = -3V$

(c) $U = -5V$ (d) $U = -7V$

(e) $U = -1V, -3V-, -5V, -7V$

Fig. 9. GS relaxation versus on reverse voltage to the SA section.

to the absorber area is inversely proportional to the output pulse width per unit time and is directly related to the pulse amplitude. In other words, as the reverse voltage increases, in fact (carrier relaxation time from the excited state to the wetting layer) in the absorber decreases, which accelerates the saturation time and emptying of the absorber. In this case, the average value of the probability of occupying the ground state in the absorber decreases. This phenomenon causes the adsorbent to be saturated in fewer time intervals and reduces the output pulse width. On the other hand, increasing the absolute value of the applied voltage increases the absorption power inside the absorber increases, which causes only higher phase modes with higher intensities to appear at the laser output. On the other hand, increasing the absolute value of the applied voltage increases the absorption power inside the absorber increases, which causes only higher phase modes with higher intensities to appear at the laser output. Under these conditions, fewer co-fuzzy modes are absorbed. As the output modes are more phased, the maximum power of the pulses will also increase. Indeed, it will not be possible to generate other co-phase modes that appear as flattened pulses. Also, changes in the applied voltage to the saturable absorber section cause changes in the ground state carrier density, which is shown in Fig. 9(a) - 9(e).

C. GS Relaxation Rate Effect on Output

Relaxation rate carrier ground state (τ_{gs}) is inversely related to the inverse voltage applied to the saturable absorber. Indeed, as the voltage applied to the absorber decreases, the value of τ_{gs} increases. At large values of τ_{gs}, its output is continuous. Phase lock occurs as the value of τ_{gs} decreases. If we reduce the weight and change the value of this time to 1 ps, as we see in Fig. 10, it goes to the Q-switching. Looking at Fig. 10, plotted for a current of 80 mA and seven different output relaxation rates, we see that changing the output time also affects the pulse width and laser output power. Indeed, with increasing this time, the output power decreases, and at the same time, the pulse width increases.

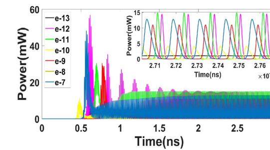

Fig. 10. Output power versus on time and for different amount of GS relaxation rate.

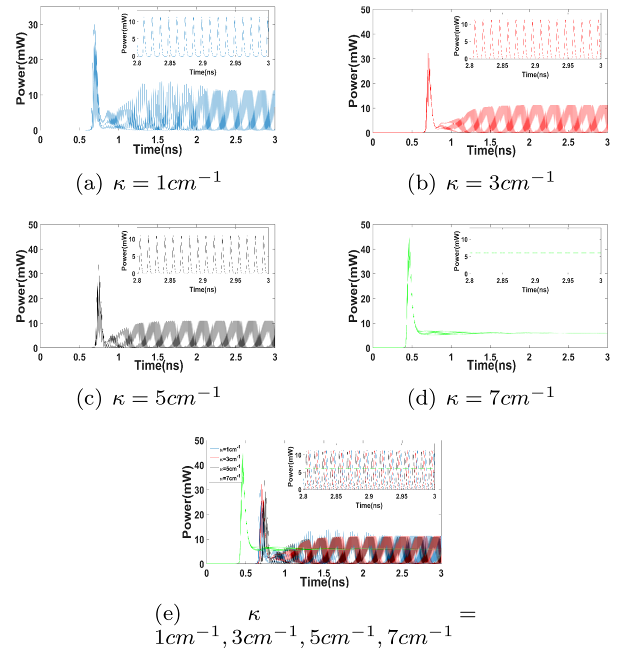

(a) $\kappa = 1cm^{-1}$ (b) $\kappa = 3cm^{-1}$

(c) $\kappa = 5cm^{-1}$ (d) $\kappa = 7cm^{-1}$

(e) $\kappa = 1cm^{-1}, 3cm^{-1}, 5cm^{-1}, 7cm^{-1}$

Fig. 11. Output power changes due to κ.

Authorized licensed use limited to: Eindhoven University of Technology. Downloaded on June 20,2022 at 13:21:18 UTC from IEEE Xplore. Restrictions apply.

D. Grating Coupling Factor (GCF)

Another important parameter of the proposed structure is the coupling factor of the backward and forward fields. The grating can be constructed in two ways—physical construction (depending on the grating shape, periodicity, refractive index contrast, etc.) and Creating a virtual effect of a physical structure in the desired area. κ in the TW model is the effective parameter of the grating. In this paper, the second method is used, which is one of the critical advantages of this structure. The basis of the grating is based on the interference of traveling waves in the absorber zone. The collision of propagating waves in the absorption region causes a static wave in the absorption region, which appears as a kappa parameter. Scaled parameter κL, where L is the grating length and κL is a dimensionless parameter that allows easy estimation of the maximal reflection provided by the grating and the width of the stopband. The following equations represent the grating created by the coupling of the fields.

$$\kappa_{E-\to+} = j\exp(-j\phi)g/2 \tag{12}$$

$$\kappa_{E+\to-} = j\exp(j\phi)g/2 \tag{13}$$

The phase of the coupling coefficient is considered as follows. In relations (12) and (13), the phase difference between the forward and backward waves is ϕ.

$$\kappa_{E+\to-} = \kappa_{E-\to+} \tag{14}$$

Indeed the most crucial difference between this article and Ref. [4] is the κ effect that is created by changes in the structure than the proposed structure in Ref. [4]. Also, contrary to what is shown in Ref. [17], the grating is embedded in the gain and absorber section; in this paper, the grating is obtained using the CPM method. A grating is created due to the collision of the forward and backward pulses in the absorber. The collision of the forward and backward pulses causes the standing wave in the absorber. In this section, we want to investigate its effect on the output pulse shape by changing this grating coefficient. Fig.11(a) -11(e) shows a graph of laser output power at 80 mA and reverse voltage of -3 volts for different coupling factor. Our simulation results shows a range of $1cm^{-1} \leq \kappa \leq 5cm^{-1}$ for pulsed laser regime. For values larger and smaller than this range, the laser's output will not be pulsed. If the laser coupling coefficient is too small, it will not light up. Also, the laser will enter the continuous wave (CW) regime for values greater than this range. On the other hand, increasing the coupling coefficient reduces the maximum laser output power. In other words, by increasing the coupling due to the greater effects of forwarding and backward waves on each other and creating stronger standing waves, we will decrease output power [24], [33]–[35].

V. Comparison Between CPM and SCPM

As mentioned earlier about using the CPM technique, the reason for using this technique was to increase the repetition rate of the output pulses. Compare two phase-locking lasers with CPM and SCPM techniques under the same conditions, which is shown Fig.12(a) Indeed, due to the rapid changes in the ground state carrier density in the CPM technique, compared to the SCPM, we will see a faster repetition rate in the output pulses. These changes in carrier density are shown in Fig.12(b) Therefore, laser output pulses with the SCPM technique have a repetition rate of about 40 GHz, and lasers with the CPM technique have about 80 GHz. This is shown in the figure below at a current of 80 mA and an absorber voltage of -3V. As shown in V, a comparison between four models of lasers with similar structures and only slightly different in terms of grating formation indicates the ability of the CPM-QDMLL laser. The current applied to the gain areas of all lasers is 1mA to 130mA, and the voltage applied to the absorber area is between 0V and -7V.

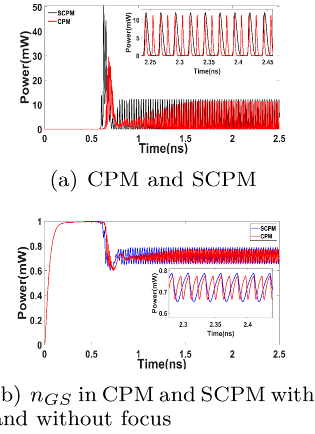

(a) CPM and SCPM

(b) n_{GS} in CPM and SCPM with and without focus

Fig. 12. Output power and probability carier density of ground state.

TABLE II
COMPARISON OF THE PARAMETERS OF FOUR SIMILAR LASER STRUCTURE MODELS IN TERMS OF QUANTUM DOTS AND DIMENSIONS

	CPM-QDMLL	SCPM-QDMLL	DFB-QDMLL	GESA-DFB-QDMLL
Power(mW)	11.42	12.05	6-9	6
Frequency(GHz)	80	40	70	88
Linewidth(ps)	2	6	6-8	6
GCF Type	Virtual Grating	-	embedded grating	embedded grating
$kappa$ parameter cm^{-1}	$1 \leq \kappa \leq 5$	-	$19 \leq \kappa \leq 21$	60

VI. Experimental Process

From the point of view of making the laser proposed in this paper, as shown in Fig. 13, the active region of laser consists of 15 layers of InAs/InGaAs QDs, with a 35 nm GaAs separating layer between each layer of QDs. Also, two layers of AlGaAs with a mole fraction of 0.35 for Al and 0.65 for Ga include layers related to quantum dots as a cladding. Buffer layers with thicknesses of 300 nm and 400 nm also surround the bottom and top cladding layers, respectively. All stages of laser fabrication can be fabricated on a GaAs substrate by S-K method using MBE and MOCVD [36]. The central wavelength of the designed structure concerning the InAs/InGaAs QDs is 1.3 μm. This wavelength range, which according to the definition of the International Telecommunication Union (ITU-T), is an excellent option for optical telecommunications used in the O-band range (1260-1360 nm) and NIR sensing applications. working wavelength range, due to the spectrum window with the least scattering in optical fibers is of great importance in urban networks, optical telecommunications and the use of pulses with high repetition rates [37]. Due to the use of InAs / GaAs quantum dots and considering the feasibility of

Authorized licensed use limited to: Eindhoven University of Technology. Downloaded on June 20,2022 at 13:21:18 UTC from IEEE Xplore. Restrictions apply.

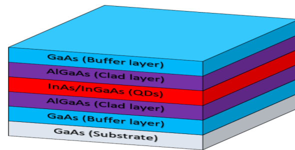

Fig. 13. Layers of laser structure proposed in fabrication process.

making such dots as QD infrared photodetectors (QDIPs) have been reported as integrated on silicon. Also, the possibility of making quantum dot lasers integrated with silicon has recently been reported, facilitating the construction of lasers proposed in the article as integrated [38]–[40].

VII. Conclusion

This article investigated a quantum dot ML laser with the CPM technique. First, by applying a current of 40 mA, the power pulses have long intervals, called the Q-switching mode. After increasing the current by 50 mA, a phase lock is performed, and the laser will have ultra-short pulses after passing an initial transient state at the output. Increasing this current to 80 mA increases the laser output power, and its pulse width decreases. Also, by increasing the absolute value of the applied reverse voltage, the output pulse width decreases. Indeed, as the voltage increases, the absorbing power of the absorber increases, and only co-phase waves that have higher energy than the other waves appear at the output. The coupling coefficient (κ) and relaxation rate carrier ground state (τ_{gs}) are two critical parameters that affect the laser output of the phase lock with the CPM technique. Increasing both of these parameters increases the pulse width, and the output power decreases. In the final part of the article, a comparison between phase lock laser with CPM technique and SCPM is performed, which shows a doubling of the repetition rate of phase lock laser with CPM structure compared to SCPM structure.

References

[1] J. Mata *et al.*, "Artificial intelligence (AI) methods in optical networks: A comprehensive survey," *Opt. Switching Netw.*, vol. 28, pp. 43–57, Apr. 2018, doi: 10.1016/j.osn.2017.12.006.

[2] S. Aleksic, "A survey on optical technologies for IoT, smart industry, and smart infrastructures," *J. Sensor Actuator Netw.*, vol. 8, no. 3, p. 47, Sep. 2019, doi: 10.3390/jsan8030047.

[3] F. Grillot, J. Duan, B. Dong, and H. Huang, "Uncovering recent progress in nanostructured light-emitters for information and communication technologies," *Light, Sci. Appl.*, vol. 10, no. 1, pp. 1–17, Dec. 2021, doi: 10.1038/s41377-021-00598-3.

[4] S. Meinecke, L. Drzewietzki, C. Weber, B. Lingnau, S. Breuer, and K. Lüdge, "Ultra-short pulse generation in a three section tapered passively mode-locked quantum-dot semiconductor laser," *Sci. Rep.*, vol. 9, no. 1, pp. 1–14, Dec. 2019, doi: 10.1038/s41598-018-38183-1.

[5] N. Ozaki *et al.*, "Integration of emission-wavelength-controlled InAs quantum dots for ultra-broadband near-infrared light source," *Nanomater. Nanotechnol.*, vol. 4, p. 26, Jan. 2014, doi: 10.5772/59315.

[6] N. Ozaki, "Noninvasive high-axial-resolution profile imaging using near infrared broadband light source based on self-assembled quantum dots," *J. Imag. Soc. Jpn.*, vol. 58, no. 6, pp. 617–625, 2019, doi: 10.11370/isj.58.617.

[7] P. Bhattacharya, A. D. Stiff-Roberts, S. Krishna, and S. Kennerly, "Quantum dot infrared detectors and sources," *Int. J. High Speed Electron. Syst.*, vol. 12, no. 4, pp. 969–994, Dec. 2002, doi: 10.1142/S0129156402001885.

[8] E. U. Rafailov, M. A. Cataluna, and W. Sibbett, "Mode-locked quantum-dot lasers," *Nature Photon.*, vol. 1, no. 7, pp. 395–401, Jul. 2007, doi: 10.1038/nphoton.2007.120.

[9] R. Rosales *et al.*, "InAs/InP quantum-dot passively mode-locked lasers for 1.55-μm applications," *IEEE J. Sel. Topics Quantum Electron.*, vol. 17, no. 5, pp. 1292–1301, Sep. 2011, doi: 10.1109/JSTQE.2011.2116772.

[10] C. Hantschmann *et al.*, "Gain switching of monolithic 1.3 μm InAs/GaAs quantum dot lasers on silicon," *J. Lightw. Technol.*, vol. 36, no. 18, pp. 3837–3842, Sep. 15, 2018, doi: 10.1109/JLT.2018.2851918.

[11] S. Lv *et al.*, "Diode-pumped continuous-wave dual-wavelength and Q-switched Yb:LuYAG lasers," *Opt. Commun.*, vol. 478, Jan. 2021, Art. no. 126356, doi: 10.1016/j.optcom.2020.126356.

[12] S. Wen *et al.*, "Dual-wavelength controllable Q-switched Nd:GSAG laser with molybdenum disulfide saturable absorber," *Infr. Phys. Technol.*, vol. 120, Jan. 2022, Art. no. 103970.

[13] H. A. Haus, "Mode-locking of lasers," *IEEE J. Sel. Topics Quantum Electron.*, vol. 6, no. 6, pp. 1173–1185, Nov. 2000, doi: 10.1109/2944.902165.

[14] L. A. Coldren, S. W. Corzine, and M. L. Mashanovitch, *Diode Lasers and Photonic Integrated Circuits*, vol. 218. Hoboken, NJ, USA: Wiley, 2012.

[15] F. Lelarge *et al.*, "Recent advances on InAs/InP quantum dash based semiconductor lasers and optical amplifiers operating at 1.55 μm," *IEEE J. Sel. Topics Quantum Electron.*, vol. 13, no. 1, pp. 111–124, Feb. 2007, doi: 10.1109/JSTQE.2006.887154.

[16] Z. Wang *et al.*, "Dual-wavelength mode-locked laser based on optimization of erbium-doped fiber length," *Optik*, vol. 251, Feb. 2022, Art. no. 168370, doi: 10.1016/j.ijleo.2021.168370.

[17] J. Rahimi, V. Ahmadi, and M. H. Yavari, "Modeling and analysis of distributed feedback quantum dot passively mode-locked lasers," *Appl. Opt.*, vol. 55, no. 19, p. 5102, Jul. 2016, doi: 10.1364/ao.55.005102.

[18] U. Bandelow, M. Radziunas, A. Vladimirov, B. Hüttl, and R. Kaiser, "40 GHz mode-locked semiconductor lasers: Theory, simulations and experiment," *Opt. Quantum Electron.*, vol. 38, nos. 4–6, pp. 495–512, Mar. 2006, doi: 10.1007/s11082-006-0045-2.

[19] E. A. Viktorov *et al.*, "Stability of the modelocking regime in quantum dot laser," in *CLEO/Eur. IQEC Conf. Dig.*, 2007, pp. 231116-1–231116-3, doi: 10.1109/CLEOE-IQEC.2007.4386957.

[20] E. A. Viktorov, P. Mandel, A. G. Vladimirov, and U. Bandelow, "Model for mode locking in quantum dot lasers," *Appl. Phys. Lett.*, vol. 88, no. 20, May 2006, Art. no. 201102, doi: 10.1063/1.2203937.

[21] R. Raghunathan *et al.*, "Pulse characterization of passively mode-locked quantum-dot lasers using a delay differential equation model seeded with measured parameters," *IEEE J. Sel. Topics Quantum Electron.*, vol. 19, no. 4, Jul. 2013, Art. no. 1100311, doi: 10.1109/JSTQE.2012.2230154.

[22] H. Wunsche, M. Radziunas, S. Bauer, O. Brox, and B. Sartorius, "Modeling of mode control and noise in self-pulsating phaseCOMB lasers," *IEEE J. Sel. Topics Quantum Electron.*, vol. 9, no. 3, pp. 857–864, May 2003, doi: 10.1109/JSTQE.2003.818854.

[23] M. Radziunas, A. G. Vladimirov, and E. A. Viktorov, "Traveling wave modeling, simulation, and analysis of quantum-dot mode-locked semiconductor lasers," *Proc. SPIE*, vol. 7720, Apr. 2010, Art. no. 77200X, doi: 10.1117/12.853825.

[24] D. J. Jones, L. M. Zhang, J. E. Carroll, and D. D. Marcenac, "Dynamics of monolithic passively mode-locked semiconductor lasers," *IEEE J. Quantum Electron.*, vol. 31, no. 6, pp. 1051–1058, Jun. 1995, doi: 10.1109/3.387042.

[25] R. G. M. P. Koumans and R. Van Roijen, "Theory for passive mode-locking in semiconductor laser structures including the effects of self-phase modulation, dispersion, and pulse collisions," *IEEE J. Quantum Electron.*, vol. 32, no. 3, pp. 478–492, Mar. 1996, doi: 10.1109/3.485400.

[26] V. Moskalenko, K. A. Williams, and E. A. J. M. Bente, "Integrated extended-cavity 1.5-μm semiconductor laser switchable between self- and anti-colliding pulse passive mode-locking configuration," *IEEE J. Sel. Topics Quantum Electron.*, vol. 21, no. 6, pp. 40–45, Nov. 2015, doi: 10.1109/JSTQE.2015.2435900.

[27] M. Radziunas, A. G. Vladimirov, E. A. Viktorov, G. Fiol, H. Schmeckebier, and D. Bimberg, "Pulse broadening in quantum-dot mode-locked semiconductor lasers: Simulation, analysis, and experiments," *IEEE J. Quantum Electron.*, vol. 47, no. 7, pp. 935–943, Jul. 2011, doi: 10.1109/JQE.2011.2142294.

[28] U. Bendelow, M. Radziunas, J. Sieber, and M. Wolfrum, "Impact of gain dispersion on the spatio-temporal dynamics of multisection lasers," *IEEE J. Quantum Electron.*, vol. 37, no. 2, pp. 183–188, Feb. 2001, doi: 10.1109/3.903067.

[29] P. Moreno *et al.*, "Intraband carrier photoexcitation in quantum dot lasers," *Nano Lett.*, vol. 8, no. 3, pp. 881–885, Mar. 2008, doi: 10.1021/nl073115a.

Authorized licensed use limited to: Eindhoven University of Technology. Downloaded on June 20,2022 at 13:21:18 UTC from IEEE Xplore. Restrictions apply.

[30] M. Radziunas, A. G. Vladimirov, E. A. Viktorov, G. Fiol, H. Schmeckebier, and D. Bimberg, "Strong pulse asymmetry in quantum-dot mode-locked semiconductor lasers," *Appl. Phys. Lett.*, vol. 98, no. 3, Jan. 2011, Art. no. 031104, doi: 10.1063/1.3544579.

[31] A. Markus *et al.*, "Two-state switching and dynamics in quantum dot two-section lasers," *J. Appl. Phys.*, vol. 100, no. 11, 2006, Art. no. 113104, doi: 10.1063/1.2397293.

[32] E. A. Viktorov *et al.*, "Recovery time scales in a reversed-biased quantum dot absorber," *Appl. Phys. Lett.*, vol. 94, no. 26, Jun. 2009, Art. no. 263502, doi: 10.1063/1.3159838.

[33] L. N. Binh, *Optical Fiber Communication Systems With MATLAB and Simulink Models*. Boca Raton, FL, USA: CRC Press, 2014.

[34] M. Radziunas, V. Z. Tronciu, E. Luvsandamdin, C. Kurbis, A. Wicht, and H. Wenzel, "Study of microintegrated external-cavity diode lasers: Simulations, analysis, and experiments," *IEEE J. Quantum Electron.*, vol. 51, no. 2, pp. 1–8, Feb. 2015, doi: 10.1109/JQE.2014.2377557.

[35] J. Carroll, J. Whiteaway, and D. Plumb, "Distributed feedback semiconductor lasers," *Physics*, 1998, doi: 10.1049/pbcs010e.

[36] M. Kuntz, "Modulated InGaAs/GaAs quantum dot lasers," Ph.D. dissertation, Technische Univ. Berlin, Berlin, Germany, 2006.

[37] E. U. Rafailov, M. A. Cataluna, and E. A. Avrutin, *Ultrafast Lasers Based on Quantum Dot Structures: Physics and Devices*. Hoboken, NJ, USA: Wiley, 2011.

[38] J. Wu *et al.*, "Monolithically integrated InAs/GaAs quantum dot mid-infrared photodetectors on silicon substrates," *ACS Photon.*, vol. 3, no. 5, pp. 749–753, May 2016, doi: 10.1021/acsphotonics.6b00076.

[39] S. Liu *et al.*, "High-channel-count 20 GHz passively mode-locked quantum dot laser directly grown on Si with 41 Tbit/s transmission capacity," *Optica*, vol. 6, no. 2, p. 128, Feb. 2019, doi: 10.1364/optica.6.000128.

[40] J. C. Norman *et al.*, "A review of high-performance quantum dot lasers on silicon," *IEEE J. Quantum Electron.*, vol. 55, no. 2, pp. 1–11, Apr. 2019, doi: 10.1109/JQE.2019.2901508.

Mohammad Heydari was born in Tehran, Iran, in 1989. He received the M.Sc. degree in electrical engineering from Shahed University, Tehran, in 2021. His research interests include the areas of nanophotonic devices specializing in the field of semiconductor and photonic crystal lasers and sensors.

Aref Rasoulzadeh Zali was born in Tabriz, Iran, in 1986. He received the B.Sc. degree in electrical engineering from Tabriz University, Tabriz, in 2010, and the M.A. degree in electrical engineering from Tarbiat Modares University, Tehran, Iran, in 2012. He is currently pursuing the Ph.D. degree. His research interests include photonic devices, such as photodetectors, lasers, and SOAs.

Reza Esmailpour Gildeh was born in Mashhad, Iran, in 1979. He received the M.Sc. degree in electrical engineering from Shahed University, Tehran, Iran, in 2020. He is currently pursuing the Ph.D. degree. His research to date has focused on bandwidth broadening in semiconductor ring lasers by optical injection and its applications.

Ali Farmani (Member, IEEE) received the B.Sc. degree in electrical engineering from the Shiraz University of Technology in 2008, the M.Sc. degree in electrical engineering from the University of Tabriz in 2010, and the Ph.D. degree in electrical engineering from Shiraz University in 2017. During his stay at Lorestan University as an Assistant Professor (2018–2021), he has mentored several B.Sc., ten M.Sc. theses, and four Ph.D. dissertations. He is the author of more than 20 ISI papers and three book chapters. His research interests are VLSI, nanoelectronics, plasmonics, and investigation of new materials for integrated photonics. He was a recipient of the fellowship for Ph.D. study at Shiraz University as an Exceptional Talent. He received the Shiraz Distinguished Ph.D. Dissertation Award for his work on plasmonic nanostructures. He was also a recipient of the Excellent Reviewer Award from Elsevier and IEEE Journals (2017–2021).

Authorized licensed use limited to: Eindhoven University of Technology. Downloaded on June 20,2022 at 13:21:18 UTC from IEEE Xplore. Restrictions apply.